

PAPER

Frustrated tunneling ionization in strong circularly polarized two-color laser fields

To cite this article: Chuanpeng Cao *et al* 2021 *J. Phys. B: At. Mol. Opt. Phys.* **54** 035601

View the [article online](#) for updates and enhancements.




IOP | ebooks™

Bringing together innovative digital publishing with leading authors from the global scientific community.

Start exploring the collection—download the first chapter of every title for free.

Frustrated tunneling ionization in strong circularly polarized two-color laser fields

Chuanpeng Cao¹, Min Li^{1,*}, Jintai Liang¹, Keyu Guo¹, Yueming Zhou¹
and Peixiang Lu^{1,2,3,*}

¹ School of Physics and Wuhan National Laboratory for Optoelectronics, Huazhong University of Science and Technology, Wuhan 430074, People's Republic of China

² Hubei Key Laboratory of Optical Information and Pattern Recognition, Wuhan Institute of Technology, Wuhan 430205, People's Republic of China

³ CAS Center for Excellence in Ultra-intense Laser Science, Shanghai 201800, People's Republic of China

E-mail: mli@hust.edu.cn and lupeixiang@hust.edu.cn

Received 18 November 2020, revised 31 December 2020

Accepted for publication 13 January 2021

Published 15 February 2021



Abstract

We study the frustrated tunneling ionization (FTI) in counter-rotating and co-rotating circularly polarized two-color (CPTC) laser fields using a classical electron ensemble method. We find that the FTI probability depends sensitively on the relative helicity and the field amplitude ratio of the two-color laser fields. The FTI probability in the counter-rotating CPTC laser fields is three orders higher than that in the co-rotating fields. In the counter-rotating CPTC laser fields, the maximal FTI probability appears at the field amplitude ratio of ~ 2.0 , while in the co-rotating CPTC laser fields it appears at the ratio of ~ 3.6 . Tracing the electron trajectories, we find that recollision-assisted recapture plays an important role for the FTI in the CPTC laser fields. We further show that the angular momentum of the Rydberg state from the FTI events can be controlled by changing the field amplitude ratio of the counter-rotating CPTC laser fields, while it is nearly unchanged in the co-rotating CPTC laser fields.

Keywords: frustrated tunneling ionization, circularly polarized two-color laser field, Rydberg state

(Some figures may appear in colour only in the online journal)

1. Introduction

When an atom or a molecule interacts with a strong laser pulse, an electron can be released via tunneling ionization or multiphoton ionization [1]. Usually, the electron motion in the strong laser field can be described by the classical three-step model [2]. In this model, the released electron wave packet oscillates in the combined laser and Coulomb fields. Subsequently, parts of the electron wave packet may be driven back to the nucleus and then be scattered by the parent ion, which is known as rescattering. The rescattering in a strong laser field triggers rich physical phenomena, such as high-order harmonic generation (HHG) [3, 4], nonsequential double ionization (NSDI) [5, 6], strong-field photoelectron holography [7–9], and frustrated tunneling ionization (FTI) [10].

In the FTI, a substantial fraction of the tunneling electrons could be driven back by the laser field and be finally recaptured by the ionic cores. Classically, those tunneling electrons cannot obtain enough drift energy from the laser fields, thus at the end of the laser field they have negative energy with considering the Coulomb potential, i.e. those electrons are finally emitted into the Rydberg state [10]. The FTI has been studied in linearly and elliptically polarized laser fields for different species of atoms, molecules, and dimers [11–21], and the FTI has also important applications in accelerating neutral atoms [22] and generating coherent extreme-ultraviolet emission [23, 24]. In the FTI process, the tunneling electron can either be directly recaptured (direct capture) by the nucleus [14] or experience a recollision with the nucleus before the recapture (recollision-assisted recapture) [15]. In LP laser fields, it was shown that the contribution of the direct capture is dominated over that of the recollision-assisted recapture [15].

* Author to whom any correspondence should be addressed.

In elliptically polarized laser pulses, the yield of the FTI events decreases dramatically with increasing the pulse ellipticity [10, 16, 17, 20]. In circularly polarized laser fields, the FTI is usually ignored because a transverse drift motion due to the rotating electric field causes the electron to spiral away from the core, suppressing the rescattering rate [10, 11].

About two decades ago, it was theoretically predicted that the rescattering plays a significant role in counter-rotating circularly polarized two-color (CPTC) laser fields [25]. Recently, the counter-rotating CPTC laser field has attracted considerable attentions [26] since it has broad applications in generating bright circularly polarized extreme ultraviolet beam [27, 28] and soft-x-ray beam [29], which enables new capabilities for many studies such as probing magnetic materials and chiral molecules. It was also found that the counter-rotating CPTC laser fields can be used to control the recollision trajectory [30–32] and the returning time interval [6] in the NSDI. More recently, the strong-field photoelectron holography has also been studied in the counter-rotating CPTC laser fields [33, 34]. Moreover, it was shown that the co-rotating CPTC laser fields can also be used to control the NSDI [35]. This means that the rescattering is important not only in counter-rotating CPTC laser fields, but also in co-rotating CPTC laser fields. However, the FTI, which is closely related to the rescattering, has not been studied in the CPTC laser fields before as far as we know.

In this paper, we study the FTI in the counter-rotating and co-rotating CPTC laser fields using the classical-trajectory Monte Carlo (CTMC) model [10, 20, 36]. We find that the FTI probability depends sensitively on the relative helicity and the relative field amplitude ratio of the CPTC laser fields. In order to understand the dependence of the FTI probability on the relative helicity and the relative field amplitude ratio, we study the distribution of the FTI events in the initial tunneling coordinates (t_0, p_\perp) within the CTMC model. We find that the recollision-assisted recapture plays an important role for the FTI in the CPTC laser fields. We also study the angular momentum of the FTI electrons in the CPTC laser fields. Our results indicate that the dominant angular momentum of the FTI electrons can be precisely manipulated by changing the field amplitude ratio of the two-color components in the counter-rotating CPTC laser fields, while in the co-rotating CPTC laser fields the dominant angular momentum of the FTI electrons is nearly unchanged.

2. Methods

We use the CTMC model to simulate the FTI process of a hydrogen atom in the counter-rotating and co-rotating CPTC laser fields. In this model, the tunneling electron wave packet is approximated by an ensemble of classical trajectories. The tunneling ionization is divided into two steps, i.e. tunneling and classical propagation. In the tunneling step, the electron tunnels through the suppressed Coulomb barrier by the laser fields. The initial momentum of the tunneling electron at the instant of tunneling is depicted by

Ammosov–Delone–Krainov (ADK) theory [37], i.e. zero longitudinal momentum parallel to the instantaneous laser field direction and a Gaussian distribution for the momentum perpendicular to the instantaneous laser field direction. The initial tunneling position is derived from Landau’s theory [38]. In the classical propagation process, the tunneling electron propagates classically in the combined Coulomb and laser fields. The motion of electron is governed by the classical Newtonian equation (atomic units are used unless stated otherwise in this paper),

$$\ddot{\mathbf{r}}(t) = -\mathbf{E}(t) - \nabla V(r). \quad (1)$$

Here, $\mathbf{E}(t)$ is the laser fields and $V(r) = -1/r$ is the Coulomb potential of the hydrogen atom. At the end of the laser pulse, we collect the electrons with negative energy, i.e. the FTI electrons. Those electrons with positive energy corresponding to the ionized electrons are removed from our analysis. The FTI electron trajectory is further calculated for an additional ten cycles to obtain the stable elliptical orbits after the laser pulse. The weight of each FTI electron trajectory is given by the ADK theory [37],

$$W(t_0, p_\perp) \propto \frac{\sqrt{2I_p}}{|E(t_0)|} \exp\left[-\frac{2(2I_p)^{3/2}}{3|E(t_0)|}\right] \exp\left[-p_\perp^2 \frac{\sqrt{2I_p}}{|E(t_0)|}\right]. \quad (2)$$

Here, t_0 is the ionization time, $E(t_0)$ is the electric field strength at the instant of t_0 , p_\perp is the initial transverse momentum, and I_p is the ionization potential. Because an electron trajectory is only determined by two independent variables, i.e. the ionization time and the initial transverse momentum, those two variables constitute the initial tunneling coordinates (t_0, p_\perp) in the CTMC model.

In our simulation, we use the CPTC laser fields, which are written as,

$$\mathbf{E}(t) = f(t) \frac{E_0}{\sqrt{\xi^2 + 1}} \{[\cos(\omega t) + \xi \cos(2\omega t)]\mathbf{e}_z + [\sin(\omega t) \pm \xi \sin(2\omega t)]\mathbf{e}_x\}, \quad (3)$$

where E_0 is the field amplitude of the laser pulse, ω is the frequency of the fundamental field and ξ is the field amplitude ratio of the two-color laser components. To minimize the nonadiabatic effect associated with the tunneling ionization [39], we have chosen a wavelength of 1600 nm for the fundamental field. In this work, we set the intensity of the pulse to be $1.5 \times 10^{14} \text{ W cm}^{-2}$. In the second term of equation (3), the case of ‘-’ corresponds to the counter-rotating CPTC laser fields and the case of ‘+’ corresponds to the co-rotating CPTC laser fields. $f(t)$ is a trapezoidal envelope which has ten fundamental field cycles in total with three cycles ramping off. We also study the FTI process in the LP laser fields in order to compare with the case of the CPTC laser fields. The intensity of the LP laser pulse is $0.8 \times 10^{14} \text{ W cm}^{-2}$ and the wavelength is 1600 nm. The polarization is along the z axis. In this paper we are interested in the angular momentum distributions of the FTI electrons. The angular momentum is calculated by $\mathbf{L} = \mathbf{r} \times \mathbf{p}$, where \mathbf{r} is the electron position and \mathbf{p} is the electron momentum at the end of the laser pulse.

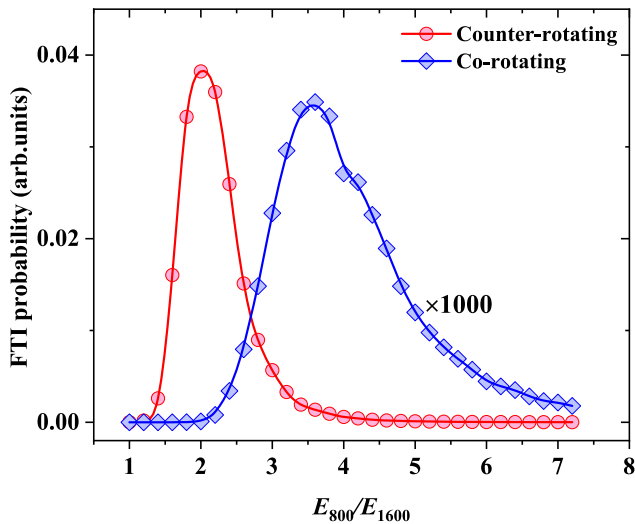


Figure 1. The FTI probability as a function of the relative field amplitude ratio (E_{800}/E_{1600}) for counter-rotating (red curve with circles) and co-rotating (blue curve with rhombus) CPTC laser fields at the intensity of $1.5 \times 10^{14} \text{ W cm}^{-2}$. The curve for the co-rotating laser fields (blue curve with rhombus) is multiplied by a factor of 1000 for visual convenience.

3. Results and discussions

Figure 1 shows the FTI probability as a function of the field amplitude ratio (E_{800}/E_{1600}) for the counter-rotating (red solid line with circles) and co-rotating (blue solid line with rhombus) CPTC laser fields at the peak intensity of $1.5 \times 10^{14} \text{ W cm}^{-2}$. Here, the FTI probability is defined as the FTI electron yield normalized to the total electrons. For both cases, the FTI probability shows a strong dependence on the field amplitude ratio of the two-color laser components. In the counter-rotating CPTC laser fields, the FTI probability reaches its maximum at $\xi = 2.0$, while in the co-rotating CPTC fields, the maximum appears at the field amplitude ratio of ~ 3.6 . We can see in figure 1 that the FTI probability in the counter-rotating CPTC laser fields is about three orders higher than that in the co-rotating laser fields. This means that the FTI probability depends sensitively on the relative helicity and the relative field amplitude ratio of the CPTC laser fields.

The field amplitude ratio corresponding to the maximum of the FTI probability is very similar to that of the NSDI probability in recent studies for both co-rotating and counter-rotating CPTC fields [30–32, 35], which means that there might be very similar electron dynamics for the FTI and NSDI in the CPTC laser fields. Because only one electron is involved in the FTI, the electron dynamics for the FTI is more easily studied, which can enrich our understanding on the NSDI in the CPTC laser fields. Next we study the electron dynamics of the FTI in the counter-rotating and co-rotating CPTC laser fields, respectively.

3.1. FTI in the counter-rotating CPTC laser field

We show the FTI electrons in the initial tunneling coordinates (t_0, p_{\perp}) in the first row of figure 2, where the second column

to the last column correspond to the results of the counter-rotating CPTC laser fields with the field amplitude ratio of 1.6, 2.0, and 2.8, respectively. The color map corresponds to the normalized yield of the FTI electrons. Varying the field amplitude ratio, the ionization time remains almost unchanged while the initial transverse momentum is dramatically changed for the FTI events. For comparison, we also show the results in the LP laser fields in figure 2(a). The distribution of the FTI events in the initial tunneling coordinates is a symmetrical crescent-shaped area for the LP laser fields [20]. However, for the counter-rotating CPTC laser fields with the field amplitude ratio of 1.6 (2.8) in figure 2(d) [figure 2(j)], only the tunneling electrons with positive (negative) initial transverse momenta can be recaptured. When the field amplitude ratio is 2.0 in figure 2(g), the distribution of the FTI electrons in the initial tunneling coordinate is similar to the case of the LP laser fields. However, there are still some differences between figures 2(a) and (g). Compared with the case of the LP laser field, more tunneling electrons with near-zero initial transverse momenta are likely to be recaptured, as shown in figure 2.

The dependence of the FTI probability on the field amplitude ratio in figure 1 can be explained qualitatively by the effect of the initial transverse momentum. With the change of the field amplitude ratio, the initial transverse momenta for the FTI events are dramatically changed. The initial transverse momenta of the FTI electrons are positive at $\xi = 1.6$ while it becomes negative at $\xi = 2.8$. At $\xi = 2.0$, the FTI electrons with near-zero initial momenta have a large contribution to the FTI probability. According to equation (2), the FTI probability is maximal at $\xi = 2.0$. This result is consistent with previous studies [26]. It demonstrated that the drift energy of the tunneling electrons in the counter-rotating CPTC laser fields changes with the field amplitude ratio, which achieves its minimum at $\xi = 2.0$. As a result, the tunneling electron at the field amplitude ratio of 2.0 will be easily to be recaptured.

We also study the angular momentum distributions of the FTI electrons, as shown in the second row of figure 2, where the color map corresponds to the angular momenta. Note that the ionization rate is not included in the second row of figure 2. The third row in figure 2 shows the angular momentum distributions of the FTI electrons. From the third row of figure 2, one knows that the dominant angular momentum is 6 (–12) for the field amplitude ratio of 1.6 (2.8). Thus the angular momentum distribution reveals a single-hump structure at the field amplitude ratio of 1.6 (2.8) in figure 2(f) [figure 2(l)], which is different from the double-hump structure for the LP laser field, as shown in figure 2(c). At the field amplitude ratio of 2.0, both positive and negative angular momenta have a large contribution to the FTI events, revealing a broad-peak structure for the distribution of the angular momenta, as shown in figure 2(i).

The results in the third row of figure 2 indicate that the angular momenta of the FTI electrons can be precisely manipulated by changing the field amplitude ratio of the two-color laser components for the counter-rotating CPTC laser fields. In the first and second rows of figure 2, one can see that the initial transverse momenta of the FTI electrons are different with varying the field amplitude ratio. Since the angular momenta of the FTI electrons is directly determined by their initial

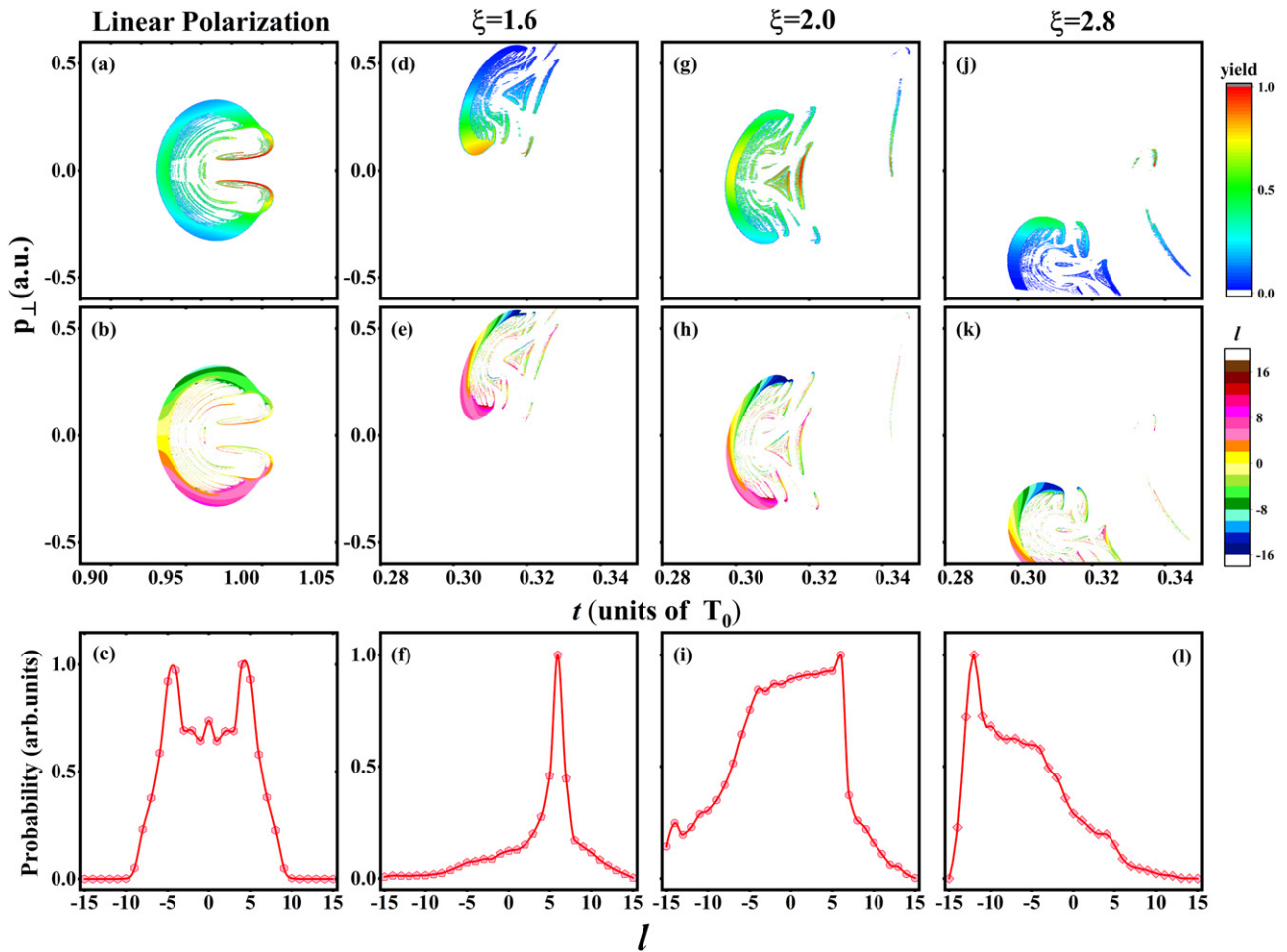


Figure 2. The first row shows the normalized yield of the FTI events in the initial tunneling coordinates (t_0, p_{\perp}) . The second row shows angular momenta of the FTI electrons in the initial tunneling coordinates. Note the ionization rate is not included in the second row. The third row shows the angular momentum distributions of the FTI electrons. The laser fields are linearly polarized (LP) laser field [(a)–(c)] and counter-rotating CPTC laser fields with $\xi = 1.6$ [(d)–(f)], 2.0 [(g)–(i)], and 2.8 [(j)–(l)], respectively. The laser intensity is $1.5 \times 10^{14} \text{ W cm}^{-2}$ for the counter-rotating CPTC laser fields and $0.8 \times 10^{14} \text{ W cm}^{-2}$ for the LP laser fields, respectively.

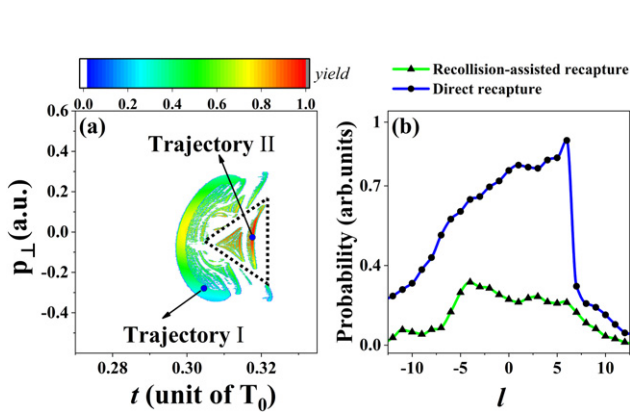


Figure 3. (a) The normalized distribution of the FTI electrons in the initial tunneling coordinate for the counter-rotating CPTC fields with $\xi = 2.0$ [the same as figure 2(g)]. The initial tunneling coordinates are separated into two regions by the dotted triangles. Trajectory I and II are selected outside and inside the dotted triangles in the initial tunneling coordinates. (b) The angular momentum distributions for different FTI electrons in figure 3(a), i.e. for recollision-assisted recapture FTI electrons (green solid line with triangles) and for direct recapture FTI electrons (blue solid line with circles).

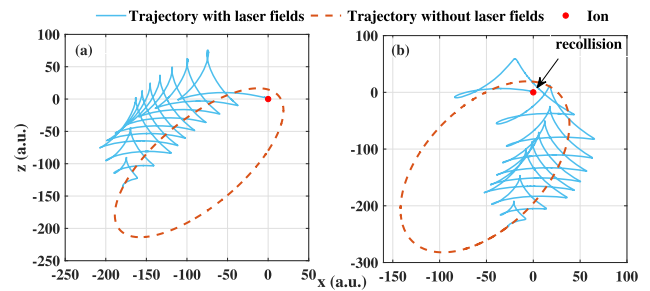


Figure 4. Typical trajectories which are selected from different regions of figure 3(a), i.e. trajectory I (a) and trajectory II (b). Red dots represent the ion. The arrow in (b) indicates the instant of recollision.

transverse momenta [20, 40], the FTI electrons obtain different angular momenta with changing the field amplitude ratio.

In order to better understand the FTI in the counter-rotating CPTC laser fields, we study the FTI electron dynamics at the field amplitude ratio of 2.0 in figures 3 and 4. In figure 3(a), the FTI events in the initial tunneling coordinates can be divided into two parts, which correspond to the regions inside and

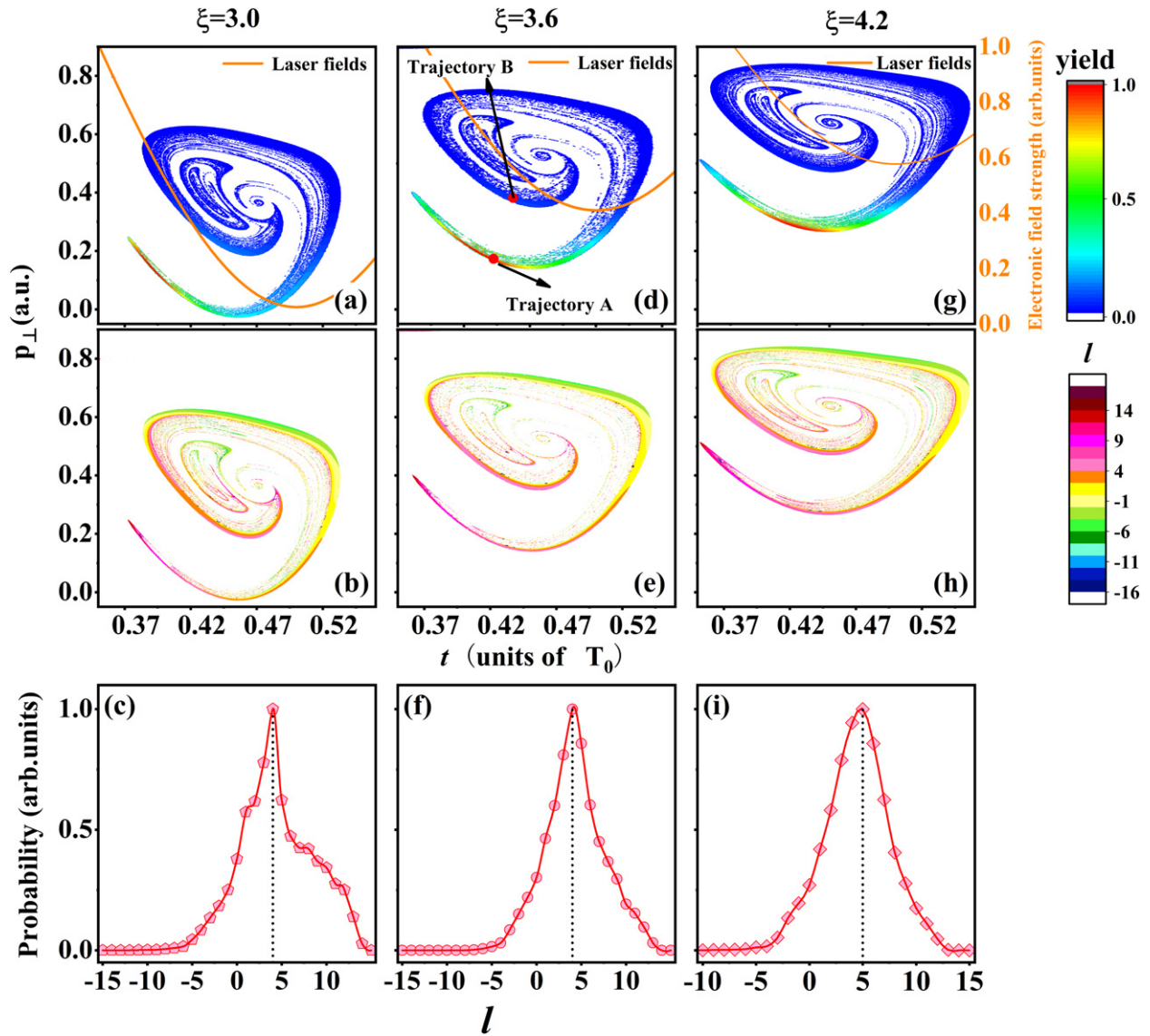


Figure 5. The first row shows the normalized yield of the FTI electrons. The orange solid lines show the laser fields in arbitrary units. The second row shows angular momenta of the FTI electrons in the initial tunneling coordinates. Note the ionization rate is not included in the second row. The third row shows the angular momentum distributions of the FTI electrons. The field amplitude ratio of the two-color laser fields are 3.0 [(a)–(c)], 3.6 [(d)–(f)], and 4.2 [(g)–(i)], respectively. The laser intensity is $1.5 \times 10^{14} \text{ W cm}^{-2}$.

outside the dotted triangle. We select typical FTI trajectory I outside the dotted triangle and trajectory II inside the dotted triangle in figure 3(a), which are shown in figures 4(a) and (b), respectively. We find that the trajectory I launches into the elliptical orbits directly as shown in figure 4(a), corresponding to direct recapture. The trajectory II in figure 4(b) experiences a recollision with the core before the recapture, corresponding to recollision-assisted recapture. Thus the FTI events inside the dotted triangle in figure 3(a) correspond to recollision-assisted recapture while the FTI events outside the dotted triangle correspond to the direct recapture. We show the angular momentum distributions of the FTI events from the recollision-assisted recapture process and the direct recapture process in figure 3(b), i.e. inside and outside the dotted triangle in figure 3(a). It is found that both recollision-assisted recapture and direct recapture have a large

contribution to near-zero angular momenta for the counter-rotating CPTC laser fields with $\xi = 2.0$. We also find that the recollision-assisted recapture constitutes $\sim 20\%$ in all recapture events at the field amplitude ratio of 2.0, which is larger than that in the LP laser fields [14, 15]. These results indicate that recollision-assisted recapture plays an important role for the FTI in the counter-rotating CPTC laser fields.

3.2. FTI in the co-rotating CPTC laser field

The results in figure 1 indicate that the FTI also exists in the co-rotating CPTC laser fields. In figure 5, we show the initial tunneling coordinates (t_0, p_{\perp}) of the FTI electrons in the co-rotating CPTC fields. The field amplitude ratios of the two-color laser components are 3.0, 3.6, and 4.2 from the first column to the third column, respectively. In the first row in figure 5, the color map shows the normalized distributions

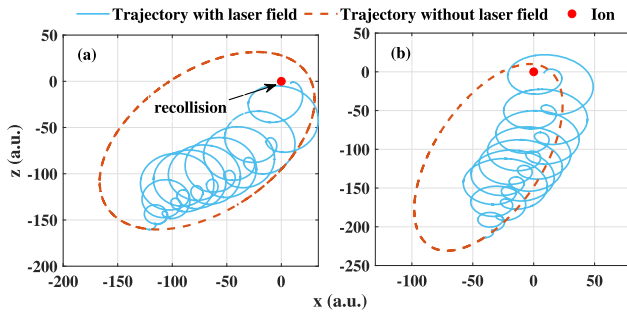


Figure 6. Typical trajectories which are selected from different regions of figure 5(d), i.e. trajectory A with small initial transverse momentum (a) and trajectory B with large initial transverse momentum (b). Red dots represents the ion. The arrow in (a) indicates the instant of recollision.

of the FTI electrons. The orange solid lines in the first row show the laser fields in arbitrary units. One can see that with changing the field amplitude ratio, both the initial transverse momenta and the ionization time of the FTI electrons are changed. On one hand, the initial transverse momenta of the FTI electrons become larger with increasing the field amplitude ratio, as shown in the first row of figure 5. This leads to a decrease of the FTI probability with increasing the field amplitude ratio according to equation (2). On the other hand, the electric field strength increases with increasing the field amplitude ratio, as shown by the orange solid lines of the first row of figure 5, which leads to an increase of the FTI probability according to equation (2). Therefore, because of the combined effect of the initial transverse momenta and the electric field strength on the ionization rate, the maximum of the FTI probability appears at the intermediate case of $\xi = 3.6$.

We also study the angular momentum distributions of the FTI electrons in the initial tunneling coordinates for the co-rotating CPTC laser fields, as shown in the second row of figure 5. In the second row of figure 5, the color map corresponds to the angular momenta of the FTI electrons. The third row in figure 5 shows the angular momentum distributions of the FTI electrons. The dominant angular momentum of the FTI electrons is approximately 4 for different field amplitude ratio. It indicates that the dominant angular momentum of the FTI electron in the co-rotating CPTC laser fields is nearly unchanged with varying the field amplitude ratio.

We also trace the trajectories of the FTI electrons with small and large initial transverse momenta in figure 6, i.e. trajectory A and trajectory B of figure 5(d). The results in figures 6(a) and (b) show that the tunneling electrons with small initial transverse momenta correspond to recollision-assisted recapture while the tunneling electrons with large initial transverse momenta correspond to direct recapture. Moreover, our results show that the recollision-assisted recapture electrons constitutes $\sim 80\%$ in all recapture events at the field amplitude ratio of 3.6. It indicates that the recollision-assisted recapture is more important for the FTI process in the co-rotating CPTC laser fields than that in the counter-rotating CPTC laser fields.

4. Conclusion

In conclusion, we have studied the electron dynamics of the FTI in the CPTC laser fields. Our results show that the FTI exists not only in the counter-rotating CPTC laser fields, but also in the co-rotating CPTC laser fields, though the FTI probability in the co-rotating CPTC laser fields is approximately three orders lower than that in the counter-rotating fields. Moreover, the FTI probability is strongly dependent on the field amplitude ratio of the two-color laser components. The FTI probability in the counter-rotating CPTC laser fields achieves its maximum at a field amplitude ratio of 2.0, while the ratio is ~ 3.6 for the co-rotating fields. Our results also indicate that the dominant angular momentum of the Rydberg state from the FTI events can be precisely manipulated by changing the field amplitude ratio of the two-color laser components in the counter-rotating laser fields, while it is slightly shifted in the co-rotating laser fields. By tracing the FTI electrons trajectories, we found that the recollision-assisted recapture process plays an important role for the FTI in both counter-rotating and co-rotating CPTC laser fields. Our study is meaningful to understand the rescattering-related process in CPTC laser fields, such as NSDI and HHG. It may be helpful to the study of Rydberg atoms in fundamental and applied physics, such as the excitation of atoms in strong laser fields [41, 42] and coherent extreme-ultraviolet emission beam generation [23].

Acknowledgments

This work was supported by National Key Research and Development Program of China (Grant No. 2019YFA0308300) and National Natural Science Foundation of China (Grant Nos. 12021004, 11722432, 11674116, and 61475055).

Data availability statement

The data that support the findings of this study are available upon reasonable request from the authors.

ORCID iDs

Chuanpeng Cao  <https://orcid.org/0000-0002-2919-6153>

Min Li  <https://orcid.org/0000-0001-7790-9739>

Keyu Guo  <https://orcid.org/0000-0001-7772-4566>

References

- [1] Protopapas M, Keitel C H and Knight P L 1997 Atomic physics with super-high intensity lasers *Rep. Prog. Phys.* **60** 389–486
- [2] Corkum P B 1993 Plasma perspective on strong field multiphoton ionization *Phys. Rev. Lett.* **71** 1994–7

- [3] Krause J L, Schafer K J and Kulander K C 1992 High-order harmonic generation from atoms and ions in the high intensity regime *Phys. Rev. Lett.* **68** 3535–8
- [4] Li L, Lan P, Zhu X, Huang T, Zhang Q, Lein M and Lu P 2019 Reciprocal-space-trajectory perspective on high-harmonic generation in solids *Phys. Rev. Lett.* **122** 193901
- [5] Watson J B, Sanpera A, Lappas D G, Knight P L and Burnett K 1997 Nonsequential double ionization of helium *Phys. Rev. Lett.* **78** 1884–7
- [6] Ma X, Zhou Y, Chen Y, Li M, Li Y, Zhang Q and Lu P 2019 Timing the release of the correlated electrons in strong-field nonsequential double ionization by circularly polarized two-color laser fields *Opt. Express* **27** 1825–37
- [7] Huismans Y *et al* 2011 Time-resolved holography with photoelectrons *Science* **331** 61–4
- [8] Tan J, Zhou Y, He M, Chen Y, Ke Q, Liang J, Zhu X, Li M and Lu P 2018 Determination of the ionization time using attosecond photoelectron interferometry *Phys. Rev. Lett.* **121** 253203
- [9] Li M *et al* 2019 Photoelectron holographic interferometry to probe the longitudinal momentum offset at the tunnel exit *Phys. Rev. Lett.* **122** 183202
- [10] Nubbemeyer T, Gorling K, Saenz A, Eichmann U and Sandner W 2008 Strong-field tunneling without ionization *Phys. Rev. Lett.* **101** 233001
- [11] Manschwetus B, Nubbemeyer T, Gorling K, Steinmeyer G, Eichmann U, Rottke H and Sandner W 2009 Strong laser field fragmentation of H₂: Coulomb explosion without double ionization *Phys. Rev. Lett.* **102** 113002
- [12] Nubbemeyer T, Eichmann U and Sandner W 2009 Excited neutral atomic fragments in the strong-field dissociation of N₂ molecules *J. Phys. B: At. Mol. Opt. Phys.* **42** 134010
- [13] von Veltheim A, Manschwetus B, Quan W, Borchers B, Steinmeyer G, Rottke H and Sandner W 2013 Frustrated tunnel ionization of noble gas dimers with Rydberg-electron shakeoff by electron charge oscillation *Phys. Rev. Lett.* **110** 023001
- [14] Landsman A S, Pfeiffer A N, Hofmann C, Smolarski M, Cirelli C and Keller U 2013 Rydberg state creation by tunnel ionization *New J. Phys.* **15** 013001
- [15] Liu H *et al* 2012 Low yield of near-zero-momentum electrons and partial atomic stabilization in strong-field tunneling ionization *Phys. Rev. Lett.* **109** 093001
- [16] Huang K, Xia Q and Fu L 2013 Survival window for atomic tunneling ionization with elliptically polarized laser fields *Phys. Rev. A* **87** 033415
- [17] Eilzer S and Eichmann U 2014 Steering neutral atoms in strong laser fields *J. Phys. B: At. Mol. Opt. Phys.* **47** 204014
- [18] Zhang W *et al* 2017 Visualizing and steering dissociative frustrated double ionization of hydrogen molecules *Phys. Rev. Lett.* **119** 253202
- [19] Dubois J, Berman S, Chandre C and Uzer T 2018 Capturing photoelectron motion with guiding centers *Phys. Rev. Lett.* **121** 113202
- [20] Zhao Y, Zhou Y, Liang J, Zeng Z, Ke Q, Liu Y, Li M and Lu P 2019 Frustrated tunneling ionization in the elliptically polarized strong laser fields *Opt. Express* **27** 0 21689
- [21] Ma J *et al* 2019 Dissociative frustrated multiple ionization of hydrogen chloride in intense femtosecond laser fields *Phys. Rev. A* **99** 023414
- [22] Eichmann U, Nubbemeyer T, Rottke H and Sandner W 2009 Acceleration of neutral atoms in strong short-pulse laser fields *Nature* **461** 1261–4
- [23] Yun H, Mun J H, Hwang S I, Park S B, Ivanov I A, Nam C H and Kim K T 2018 Coherent extreme-ultraviolet emission generated through frustrated tunnelling ionization *Nat. Photon.* **12** 620–4
- [24] Mun J H, Ivanov I A, Yun H and Kim K T 2018 Strong-field-approximation model for coherent extreme-ultraviolet emission generated through frustrated tunneling ionization *Phys. Rev. A* **98** 063429
- [25] Milošević D B, Becker W and Kopold R 2000 Generation of circularly polarized high-order harmonics by two-color coplanar field mixing *Phys. Rev. A* **61** 063403
- [26] Mancuso C A *et al* 2016 Controlling electron-ion rescattering in two-color circularly polarized femtosecond laser fields *Phys. Rev. A* **93** 053406
- [27] Fleischer A, Kfir O, Diskin T, Sidorenko P and Cohen O 2014 Spin angular momentum and tunable polarization in high-harmonic generation *Nat. Photon.* **8** 543–9
- [28] Kfir O *et al* 2015 Generation of bright phase-matched circularly-polarized extreme ultraviolet high harmonics *Nat. Photon.* **9** 99–105
- [29] Fan T *et al* 2015 Bright circularly polarized soft x-ray high harmonics for x-ray magnetic circular dichroism *Proc. Natl Acad. Sci. USA* **112** 14206–11
- [30] Chaloupka J L and Hickstein D D 2016 Dynamics of strong-field double ionization in two-color counterrotating fields *Phys. Rev. Lett.* **116** 143005
- [31] Eckart S *et al* 2016 Nonsequential double ionization by counter-rotating circularly polarized two-color laser fields *Phys. Rev. Lett.* **117** 133202
- [32] Mancuso C A *et al* 2016 Controlling nonsequential double ionization in two-color circularly polarized femtosecond laser fields *Phys. Rev. Lett.* **117** 133201
- [33] Li M, Jiang W-C, Xie H, Luo S, Zhou Y and Lu P 2018 Strong-field photoelectron holography of atoms by bicircular two-color laser pulses *Phys. Rev. A* **97** 023415
- [34] Ke Q, Zhou Y, Tan J, He M, Liang J, Zhao Y, Li M and Lu P 2019 Two-dimensional photoelectron holography in strong-field tunneling ionization by counter rotating two-color circularly polarized laser pulses *Opt. Express* **27** 0 32193
- [35] Huang C, Zhong M and Wu Z 2019 Nonsequential double ionization by co-rotating two-color circularly polarized laser fields *Opt. Express* **27** 7616
- [36] Chen J, Liu J, Fu L B and Zheng W M 2000 Interpretation of momentum distribution of recoil ions from laser-induced nonsequential double ionization by semiclassical rescattering model *Phys. Rev. A* **63** 011404
- [37] Ammosov M V, Delone N B and Krainov V P 1986 Tunnel ionization of complex atoms and atomic ions in electromagnetic field *Proc. SPIE-Int. Soc. Opt. Eng.* **64** 1181
- [38] Landau L and Lifshitz E 2013 *Quantum Mechanics: Non-relativistic Theory* (Amsterdam: Elsevier)
- [39] Liu K, Luo S, Li M, Li Y, Feng Y, Du B, Zhou Y, Lu P and Barth I 2019 Detecting and characterizing the nonadiabaticity of laser-induced quantum tunneling *Phys. Rev. Lett.* **122** 053202
- [40] Liang J, Zhang R, Ma X, Zhou Y and Lu P 2018 Angular momentum distribution in strong-field frustrated tunneling ionization *Chin. Opt. Lett.* **16** 040202
- [41] Zhang W *et al* 2019 Electron–nuclear correlated multiphoton-route to Rydberg fragments of molecules *Nat. Commun.* **10** 757
- [42] Venzke J, Gebre Y, Becker A and Jaroń Becker A 2020 Pathways to excitation of atoms with bicircular laser pulses *Phys. Rev. A* **101** 053425